

NUMERICAL SIMULATION OF ALGAS/GAAS P-I-N QUANTUM WELL SOLAR CELL

SAMIRA LAZNEK, AFEK MEFTAH, AMJAD MEFTAH, NOURDINE SENGOUGA

Laboratory of semiconducting and metallic materials (LMSM), University of Biskra BP 145, Algeria

Laznek_samira@yahoo.fr

ABSTRACT

This paper deals with a AlGaAs/GaAs p-i-n quantum well solar cell. The doped region are based on AlGaAs semiconductor while the intrinsic region "i" contain multi quantum well (MQW) system AlGaAs/GaAs. A numerical method is developed to determine the influence of insertion of MQW into the depletion region over the p-i(MQW)-n $\text{Al}_x\text{Ga}_{1-x}\text{As}$ solar cells. Current-voltage (J-V) characteristics is generated for the AM1.5 solar spectrum. The effect of the Aluminum molar fraction x ($\text{Al}_x\text{Ga}_{1-x}\text{As}$), the number, the width, the depth of the wells and barriers in the "i" layer and the doping densities on the electrical outputs and the quantum efficiency of the solar cell are also presented. The optimized solar cell reached a conversion efficiency of 28.72 % with a short circuit current density of 36.9 mA/cm² and an open circuit voltage of 0.97 V.

KEYWORDS: Quantum well; Solar cell; AlGaAs; Conversion efficiency; Modeling.

1 INTRODUCTION

A quantum well solar cell (QWSC) is a multi-band gap solar cell which encloses multi-quantum well layers in the intrinsic region of a p-i-n structure figure (1). The use of quantum wells to improve solar cell efficiencies was at first proposed by Barnham and Duggan [1]. The intrinsic region is useful to extend the field-bearing region. In addition the i-region of the p-i-n solar cell structure consists of a number of wells that have an energy gap narrower than the one of the p-i-n basic material. This allows the absorption of the low-energy photons in the wells and the photoresponse of the cell can be increased to longer wavelengths.

Different theoretical models were proposed to simulate the operating mode of QWSCs depending on the well's parameters (number, depth, widths, barriers....) [2-5]. The output voltage of the QWSC is dominated by the wider band gap barrier material and the recombination in the wells and in the interfaces between barriers and wells materials. The absorption, the spectral response and hence short circuit current are determined by the width and depth of the quantum well [5-6]. The short-circuit current is improved because of the additional absorption of low-energy photons in the lower band-gap quantum wells while recombination of carriers trapped in the quantum wells can reduce the open-circuit voltage [7]. Fortunately, experimental results have shown that the supplementary photocurrent resulting from the extension of the absorption spectrum to lower energies can compensate the associated

decrease in the open-circuit voltage [7-8-9].

In this study we have adopted theoretical models of Anderson et al [4] and Rimada et al [5-7] to calculate the quantum efficiency and the short circuit current density which is the maximum photocurrent generated by the QWSC under light. The considered light is the AM1.5, which is common to characterizing terrestrial solar spectrum. Then to calculate the full J-V characteristic we have developed our own program under MATLAB language.

Firstly Schrödinger equation is solved numerically to determine the confined energy states in a single quantum well; the second step consists of calculating the absorption coefficient taking into account the allowed valence to conduction bands transitions. Finally the total photocurrent is analyzed for various structure parameters specifically; width, height (related to the Aluminum concentration), number of wells inside the intrinsic layer, and the doping densities.

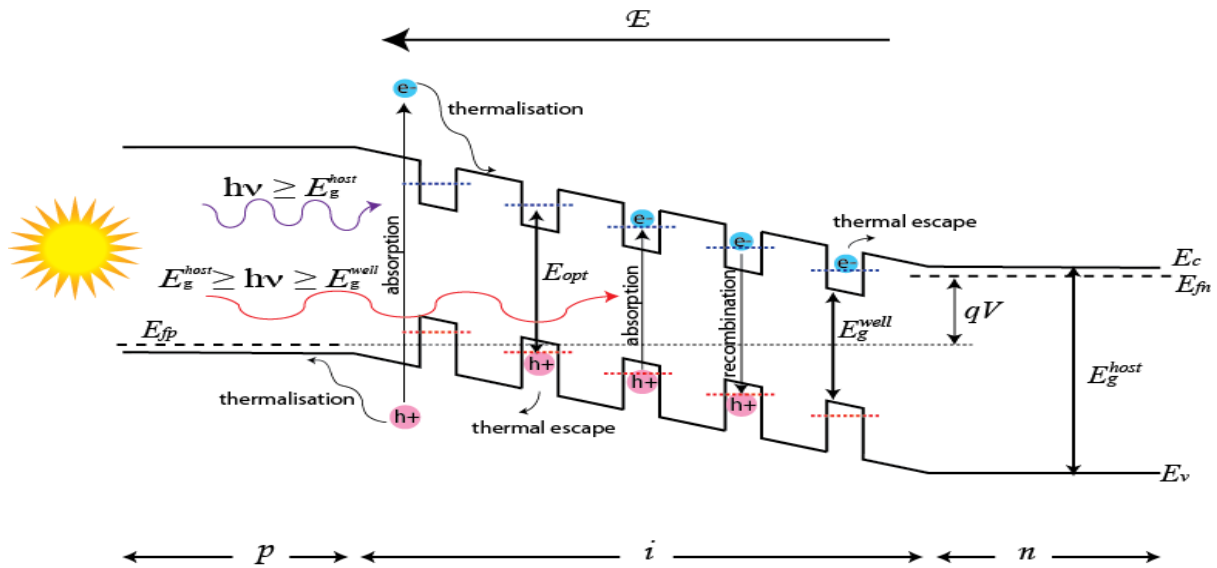


Figure 01: p-i(MQW)-n solar cell

2 THEORETICAL MODEL

We have considered a QWSC with N_w wells each of length L_w in the intrinsic region of length W with a barrier band gap E_B and a well band gap E_w . The wells and barriers are each constructed from $Al_xGa_{1-x}As$, $0 \leq x \leq 0.35$. Rimada's current- voltage relation is then [5-6,10] :

$$J(V) = J_0(1 + r_R \beta) \left[\exp\left(\frac{qV}{kT}\right) - 1 \right] + (r_{RN} \alpha + J_s) \left[\exp\left(\frac{qV}{2kT}\right) - 1 \right] - J_{PH} \quad (1)$$

where

$$r_R = 1 + f_w \left[\gamma_{BYDOS}^2 \exp\left(\frac{\Delta E}{kT}\right) - 1 \right] \quad (2.a)$$

$$r_{NR} = 1 + f_w \left[\gamma_{BYDOS} \exp\left(\frac{\Delta E}{2kT}\right) - 1 \right] \quad (2.b)$$

Are the radiative and ‘non-radiative enhancement ratio, respectively, and represent the increment in the net intrinsic region radiative and non-radiative recombinations due to the insertion of the quantum wells. The J_s is the surface recombination current. The term J_s was introduced to represent the well-barrier interface recombination, which is characterized by the recombination velocity v_s [5-6,10] :

$$J_s = 2Nqn_{iB}v_s\gamma_{DOS} \exp\left(\frac{\Delta E}{kT}\right) \quad (3)$$

Here, $\Delta E = E_B - E_A$, and all the terms in equation (1) and (2) are identical to reported ones by Anderson [5-6,10]. The photocurrent J_{PH} is calculated from the external quantum efficiency of the cell (QE). The p-region and n-region

contribution was classically evaluated solving the carrier transport equations. The contribution of photo-generated carriers in the intrinsic region to QE values is calculated by the following expression :

$$QE(\lambda) = (1 - R(\lambda)) \exp\left\{ \left(\sum_i \alpha_i z_i \right) \right\} \times (1 - e^{-\alpha_B W - N_w \alpha_w^*}) \quad (4)$$

Where $R(\lambda)$ is the surface reflectivity spectrum of the antireflection coating. The first exponential factor is due to the attenuation of light in the precedent layers of the cell, α_i and z_i are the absorption coefficient and the width of the precedent layers, respectively, the α_B is the absorption coefficient of the bulk barrier material, N_w is the number of wells and α_w^* is the non-dimensional quantum well absorption, used for energies below the barrier band gap. Following Bastard [11], we calculate the density of states for the single quantum well within the envelope function approximation. When mixing between light and heavy Valence sub-bands is neglected, the well absorption coefficient can be calculated as follows:

$$\alpha_w^*(E) = \alpha_w t \quad (5)$$

$$\alpha_w(\lambda) = \sum \alpha_{e_n - \hbar k_m} + \sum \alpha_{e_n - l \hbar m} \quad (6)$$

$$\alpha_{e_n-hh_m} = \frac{\pi q^2 E_P}{4\pi \epsilon_0 n_r C m_0 E_n \ell \hbar} \frac{m_{e,W} m_{hh,W}}{m_{e,W} + m_{hh,W}} |\langle \psi_n^e | \psi_m^{hh} \rangle|^2 [\Theta(E - E_n) + |f_i|^2 \delta(E - E_n)] \quad (7 - a)$$

and

$$\alpha_{e_n-lh_m} = \frac{\pi q^2 (E_P/3)}{4\pi \epsilon_0 n_r C m_0 E_n \ell \hbar} \frac{m_{e,W} m_{lh,W}}{m_{e,W} + m_{lh,W}} |\langle \psi_n^e | \psi_m^{lh} \rangle|^2 [\Theta(E - E_n) + |f_i|^2 \delta(E - E_n)] \quad (7 - b)$$

where $\sum \alpha_{e_n-hh_m}$ and $\sum \alpha_{e_n-lh_m}$ are the absorption coefficients due to electron-heavy hole and electron-light hole transitions to conduction band, respectively, α_w is the well absorption coefficient, E_n are the transition energies, ℓ is the quantum thickness of the heterostructure and all other symbols have their usual definitions[11]. The transition energies of quantum wells can be calculated by solving the Schrödinger equation for the electrons and holes in the potential wells created by band discontinuities. The sub band energies are calculated by solving self-consistently the one-dimensional Poisson-Schrödinger equations within the effective mass approximation.

The nonlinear Poisson equation for the electrostatic potential Φ is:

$$\frac{\partial}{\partial z} \left(\epsilon \frac{\partial \Phi(z)}{\partial z} \right) = -e(p(z) - n(z) + N_D^+ - N_A^-) = -\rho(z) \quad (8)$$

Where ϵ is dielectric constant, $\rho(z)$ is the charge density, e is the electron charge, n and p are the electron and hole concentrations, and N_D^+ and N_A^- are the ionized donors and acceptors concentrations. In the case of strong confinement in only one direction, we assume that the density of states can be decomposed in a quantum term along the confined direction (z) and semi-classical term in the other directions. The one-dimensional Schrödinger equation for electrons in the z direction can be written as :

$$-\frac{\hbar^2}{2} \frac{\partial}{\partial z} \left(\frac{1}{m_g} \frac{\partial \psi_{i_s, i_{hh}, i_{lh}}(z)}{\partial z} \right) + V(z) \psi_{i_s, i_{hh}, i_{lh}}(z) = E_{i_c, i_{hh}, i_{lh}} \psi_{i_s, i_{hh}, i_{lh}}(z) \quad (9)$$

where ψ_i represent the wave function in the conduction and valence bands, E_{i_c} $E_{i_{hh}}$ $E_{i_{lh}}$ are the corresponding eigenvalues and m_e , m_{hh} , m_{lh} are the effective masses.

The photocurrent was calculated from integration of external efficiency of the cell oversolar spectrum in AM1.5 solar radiation [12] :

$$J_{PH} = q \int F(\lambda) Q E_{TOT}(\lambda) d\lambda \quad (10)$$

Where $F(\lambda)$ is the AM1.5 solar spectrum photon flux ($cm^{-2} s^{-1}$).

And then, Equation (1) is completely determined. The short-circuit current and open-circuit voltage, respectively, for the solar cell are determined by :

$$J_{SC} = J_{PH} \quad (11)$$

$$V_{OC} = \frac{kT}{e} \ln \left(\frac{J_{SC} + J_0 (1 + r_R \beta)}{J_0 (1 + r_R \beta)} \right) \quad (12)$$

The efficiency of the solar cell given by :

$$\eta = \frac{V_m J_m}{P_{in}} \times 100\% \quad (13)$$

Where $P_{in} = 1000 W m^{-2}$ is the input power from the sunlight for 1-sun under 1.5 condition. Here J_m is the current corresponding to maximum power output, which is obtained by derivation of $P = JV$ with respect to current density J and setting $\partial P / \partial J = 0$ [3]. V_m is obtained by solving the equation using the iteration procedure :

$$\exp \left(\frac{V_m}{V_T} \right) \left[1 + \frac{V_m}{V_T} \right] = \exp \left(\frac{V_{OC}}{V_T} \right) \quad (14)$$

where ($V_T = kT/e$) is the thermal voltage. Another important solar parameter is the fill factor (FF), which measures the squareness of the photo-J-V curve, defined by :

$$FF = \frac{V_m J_m}{V_{OC} J_{SC}} \quad (15)$$

3 RESULTS AND DISCUSSIONS

To model the p-i(MQW)-n solar cells figure (2), we have considered a structure that includes a ZnS anti-reflection coating layer with 65 nm thickness, a cap layer with 0.02 μm thickness, the p- $Al_x Ga_{1-x} As$ layer and n- $Al_x Ga_{1-x} As$ layer with 0.15 and 0.46 μm thickness. In addition we have assumed that the n-region and p-region are uniformly doped

with $N_{A,p} = N_{D,n} = 10^{18} \text{ cm}^{-3}$, respectively. The intrinsic region is formed by GaAs quantum wells and $\text{Al}_x\text{Ga}_{1-x}\text{As}$ barriers. Other physical parameters of material used in the

calculation are presented in the table(1).

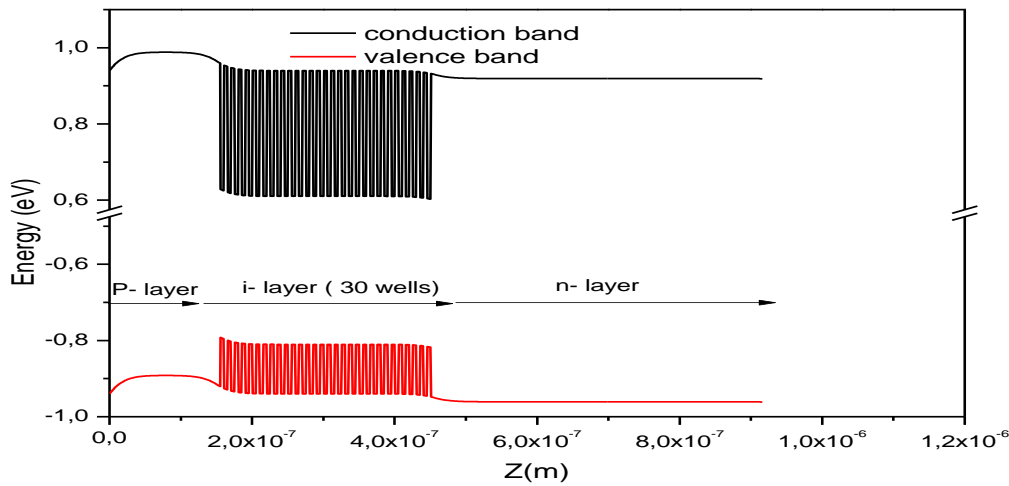


Figure 02: The energy band diagram of an optimized MQW cell

Table 01: Material parameters used for modeling the AlGaAs/GaAs QWSCs

Parameters	Analytic expressions	References
Absorption coefficient	$\alpha_x(\lambda) = \alpha_{\text{GaAs}}(\lambda')$ $E = hc/\lambda$ $E - E_g(x) = E' - E_g(0) - 0.62x [E - E_g(0)]^{0.5}$	[13]
Dielectric constant	$\epsilon = (13.1 - 2.2x)\epsilon_0$	[14]
Mobility	$\log_{10}(\mu_e) = \left[\frac{-1.5545 + 0.0016 + (0.735 + 0.0013x)\log_{10}(N_a)}{-(0.0253 + 0.0052x)\log_{10}[(N_a)]^2} \right] \left(\frac{300}{T} \right) \left(\frac{\text{cm}^2}{V_s} \right)$ $\log_{10}(\mu_h) = \left[\frac{-9.723 + 0.0095 + (1.576 + 0.0012x)\log_{10}(N_d)}{-(0.0507 + 0.0034x)\log_{10}[(N_d)]^2} \right] \left(\frac{300}{T} \right)^{\frac{3}{4}} \left(\frac{\text{cm}^2}{V_s} \right)$	[14]
Diffusion length	$L_e = \left[\frac{\mu_e(N_a, x)}{\mu_e(N_a, 0)} \right] \exp(-9.72x) \left[\frac{-210.06 + 27.254\log_{10}(N_a)}{-0.850\log_{10}[(N_a)]^2} \right] \left(\frac{300}{T} \right)^{0.97} \mu\text{m}$ $L_h = \left[\frac{\mu_h(N_d, x)}{\mu_h(N_d, 0)} \right] \exp(-9.72x) \left[\frac{-116.92 + 14.466\log_{10}(N_d)}{-0.438\log_{10}[(N_d)]^2} \right] \left(\frac{300}{T} \right) \mu\text{m}$	[14]

Effective masses	$m_e = (0.0632 + 0.0856x + 0.0231x^2)m_0$ $m_{ih} = (0.088 + 0.0375x + 0.0163x^2)m_0$ $m_{hh} = (0.50 + 0.2x)m_0$	[15]
------------------	---	------

3.1 Effect of Al molar fractions in the barriers

The J-V curves for different solar cells with different i-region structures that include different Al molar fractions in the barriers are investigated. In this case, the considered number of the wells is $N_w=50$ with a well width of $L_w=15\text{nm}$ and a barrier width of $L_b=10\text{nm}$. The Al fraction molar is increased from 0.1 to 0.3. Fig. 3 shows, that with increasing the Al molar fractions in the barriers, the short circuit current in the intrinsic region reduces faster than open circuit voltage. The extracted output parameters are presented in table (2) and Fig. 4.

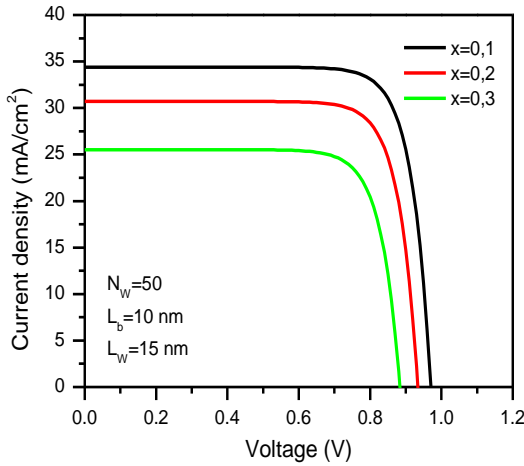


Figure 03: The effect of the Al molar fractions in the barriers on solar cell J-V characteristics

Table 02: The Al molar fractions in the barriers effect on solar cell output parameters

Al molar fractions	$J_{sc} (mA/cm^2)$	$V_{oc} (V)$	FF%	$\eta\%$
0.1	34.39	0.97	79.90	26.65
0.2	30.70	0.93	79.68	22.75
0.3	25.52	0.88	78.83	17.70
Al molar fractions	$J_{sc} (mA/cm^2)$	$V_{oc} (V)$	FF%	$\eta\%$
0.1	34.39	0.97	79.90	26.65
0.2	30.70	0.93	79.68	22.75
0.3	25.52	0.88	78.83	17.70

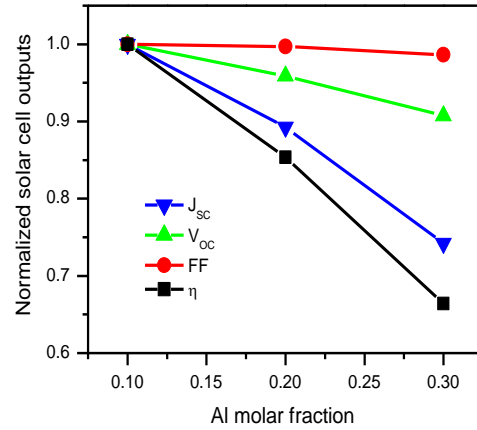


Figure 04: The effect of the Al molar fractions in the barriers on the solar cell output parameters

From the obtained results, the output parameters of the cell decrease with the increase of the Al molar fraction. J_{sc} and η are the more affected while V_{oc} and FF decreases lightly. The depth of the well ΔE is related to the Al fraction molar. When there is an increase of Al molar fractions in the barriers, ΔE increases and induces an increase in the recombination (Eq.2). The other parameter influenced by the Al molar fraction is the absorption coefficient in the quantum wells. Fig. 5 shows the effect of Al molar fraction in the absorption coefficient. As depicted in the figure, with increasing the Al molar fractions in the barriers, the absorption coefficient decreases and shifts toward shorter wavelengths. The increase of the recombination and the decrease of the absorption can explain the reduction of the cell output parameters, namely J_{sc} and V_{oc} .

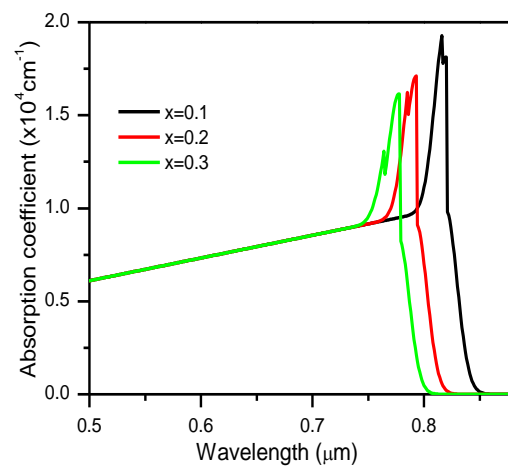


Figure 05: The effect of the Al molar fraction in the barriers on absorption coefficient

3.2 Effect of the barrier width

In this section, the effect of the barrier width layer is studied. Fig. 6 shows the I-V characteristics simulated when the barrier width layer is reduced from 15 to 1 nm. The extracted output parameters are presented in table (3) and Fig. 7.

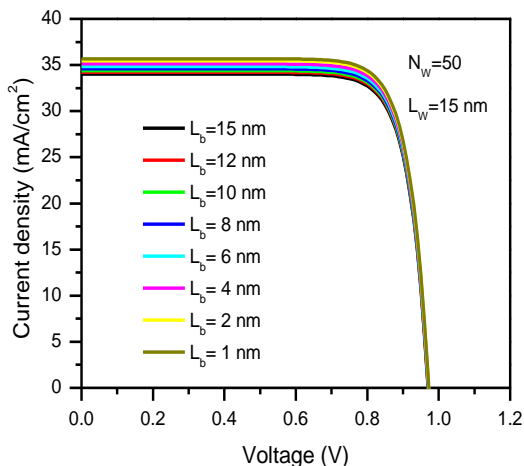


Figure 06: The barriers width effect on solar cell I-V characteristics

Table 03: The barriers width effect on solar cell output parameters

The barriers width (L _b)	$J_{sc} (mA/cm^2)$	$V_{oc} (V)$	FF%	η %
15	34.01	0.97	79.85	26.34
12	34.22	0.97	79.88	26.51
10	34.39	0.97	79.90	26.65
08	34.59	0.97	79.93	26.82
06	34.83	0.97	79.96	27.01
04	35.12	0.97	80.00	27.25
02	35.47	0.97	80.05	27.54
01	35.68	0.97	80.08	27.71

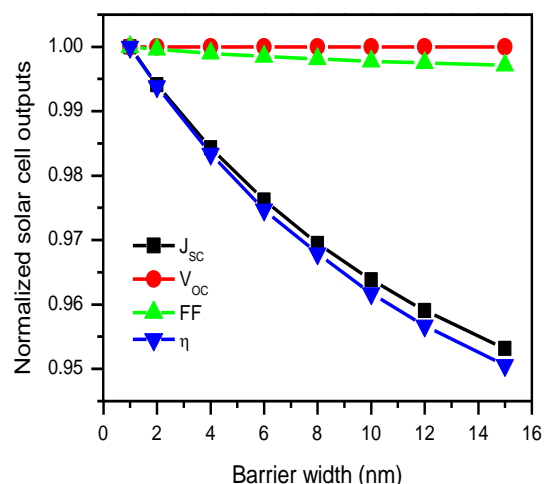


Figure 07: The barrier width effect on the solar cell output parameters

As we can see from the obtained results, a weak sensitivity of the output parameters to the barrier width increase from 1 to 15 nm is observed, namely occurs in J_{sc} and η .

3.3 Effect of the well numbers

In this section, the effect of the number of the wells is investigated. Fig. 8 shows the J-V characteristics simulated when the number of wells were varied from 50 to 10. The extracted output parameters are presented in table (4) and Fig. 9.

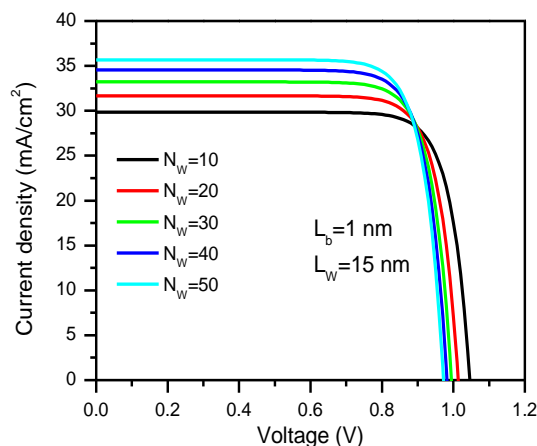
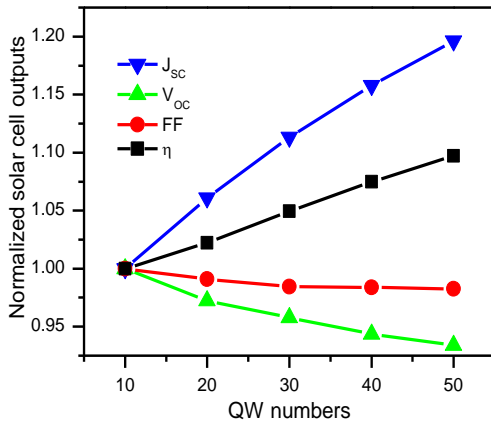


Figure 08: The QWs effect on solar cell J-V characteristics

Table 04: The QWs number effect on solar cell output parameters

Number of wells	$J_{sc} \text{ (mA/cm}^2\text{)}$	$V_{oc} \text{ (V)}$	FF%	$\eta\%$
10	29.83	1.044	81.09	25.26
20	31.65	1.015	80.35	25.82
30	33.21	1.000	79.82	26.51
40	34.54	0.985	79.79	27.15
50	35.68	0.975	79.67	27.71


Figure 09: The QW number effect on solar cell output parameters

From the obtained results, all output parameters are sensitive to the number of quantum wells in the intrinsic region. J_{sc} increases significantly from 29.83 to 35.86 mA/cm^2 . The conversion efficiency η reaches 27.71 % for 50 wells. However, V_{oc} decreases slowly from 1.044 to 0.975 V and FF follows V_{oc} variations by decreasing to 79.67%. Then there is a difference between the behavior of J_{sc} (η) and that of V_{oc} (FF). It seems that the increase of the well numbers motivates the transfer of the free carriers between the wells at the expense of the potential.

3.4 Effect of the well width:

Fig. 10 shows the effect of the quantum well width (L_w) on the J-V characteristics for two different well depth ($\Delta E=133$ meV and $\Delta E=450$ meV). The extracted outputs are summarized in table (5). We observe that the increase of the quantum well width from 1nm to 10 nm improves J_{sc} and this improvement is more pronounced for the deeper well ($\Delta E=450$ meV).

This is a consequence of the quantum nature of photon absorption in the wells. For small barrier heights, the number of levels in the well does not change significantly with the increase in the quantum well width. Then, for larger barrier heights, the number of levels and amount of transition enlarge with the increase of the quantum well width leading to a greater absorption of the incident photons and therefore an increase in short circuit current density.

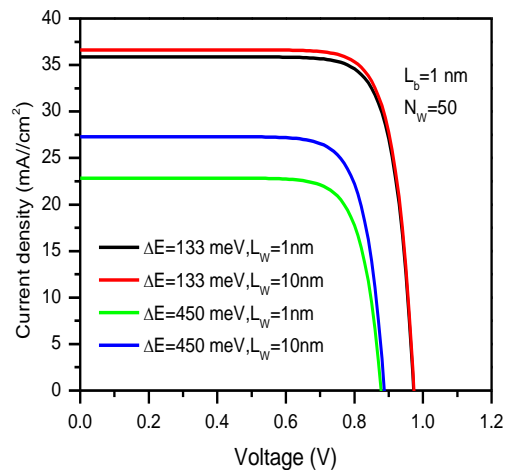

Figure 10: The well width effect on the solar cell J-V characteristics

Table 05: The well depth and width effect on solar cell output parameters

Well depth and width	$J_{sc} (mA/cm^2)$	$V_{oc} (V)$	$FF\%$	$\eta\%$
$\Delta E=133$ meV, 1nm	22.84	0.87	79.11	15.72
$\Delta E=133$ meV, 10nm	27.27	0.88	79.18	19.01
$\Delta E=450$ meV, 1nm	35.87	0.97	80.11	27.87
$\Delta E=450$ meV, 10nm	36.63	0.97	80.22	28.50

3.5 Effect of doping concentrations

In this section, the effect of the doping densities in n (N_d) and p-layers (N_a) is studied. Fig. 11 shows the J-V characteristics simulated when N_d and N_a are varied from 10^{16} to 10^{18} cm^{-3} . The extracted output parameters are presented in table (6) and Fig. 12.

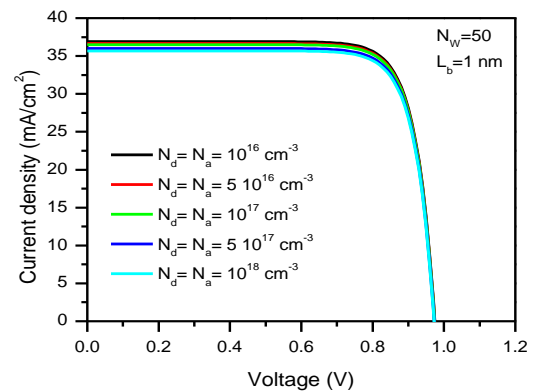


Figure 11: The p and n –region doping concentration effect on the solar cell J-V characteristics

Table (6) The p and n –region doping concentration effect on the solar cell output parameters

P and n-region doping (cm^{-3})	$J_{sc} (mA/cm^2)$	$V_{oc} (V)$	$FF\%$	$\eta\%$
10^{16}	36.90	0.97	80.26	28.72
$5 \cdot 10^{16}$	36.65	0.97	80.23	28.52
10^{17}	36.50	0.97	80.20	28.39
$5 \cdot 10^{17}$	36.00	0.97	80.13	27.98
10^{18}	35.68	0.97	80.00	27.71

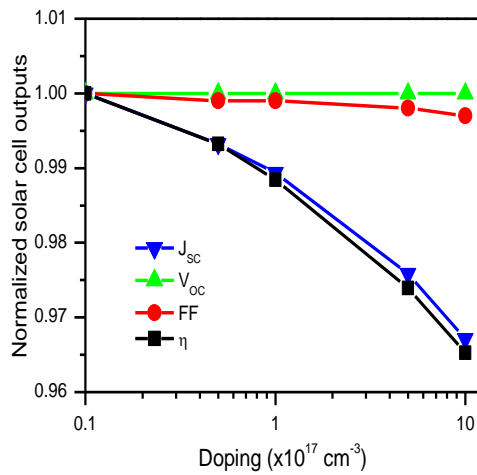


Figure 12: The p and n -region doping concentration effect on solar cell output parameters

The obtained results indicate slight effect of the doping densities increase on the outputs of the cell. V_{oc} and FF seem to be insensitive to the increased of doping concentration. J_{sc} decreases slightly from 36.90 to 35.68 mA/cm^2 , and η follows J_{sc} variations and decrease from 28.72 to 27.71%.

3.6 Effect of the well-barrier interface recombination

In this section, the effect of the well-barrier interface recombination velocity is investigated. Fig. 13 shows the J-V characteristics simulated when the recombination velocity is increased from 30 to 300 cm/s . The extracted output parameters are summarized in table (6) and presented graphically in Fig. 14.

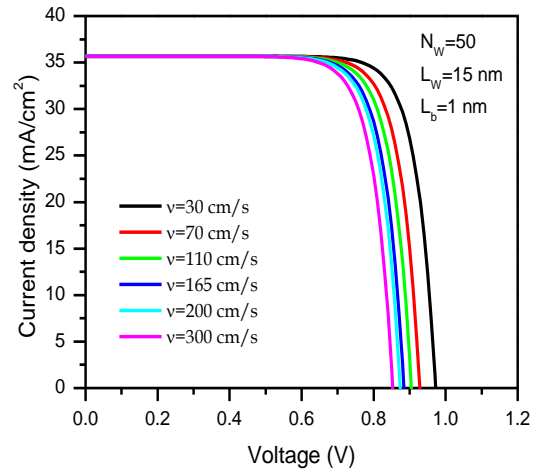


Figure 13: The interface recombination effect on solar cell I-V characteristics

Table (6) The interface recombination effect on solar cell output parameters

Interface recombination (cm/s)	$J_{sc} (\text{mA/cm}^2)$	$V_{oc} (V)$	FF%	$\eta\%$
30	35.68	0.97	80.08	27.71
70	35.68	0.92	79.95	26.24
110	35.68	0.90	79.31	25.47
165	35.68	0.88	78.88	24.77
200	35.68	0.87	78.71	24.43
300	35.68	0.85	78.26	23.73

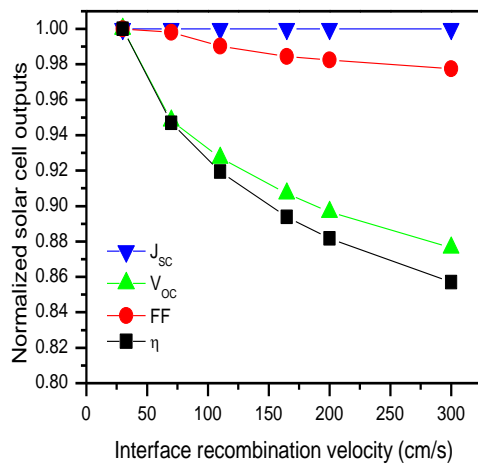


Figure 14: The interface recombination effect on solar cell output parameters

We can see the obtained results indicated that there is a slow decrease in FF as the interface recombination is increased. However, J_{sc} seems to be surprisingly insensitive to the increased of interface recombination. V_{oc} decreases from 0.97 to 0.85V, and the efficiency η follows the V_{oc} variations by decreasing to 23.73%.

We finish this section by the examination of the effect of the barrier band gap energy E_b for three different recombination velocity on the cell efficiency η . The result is shown in Fig.15, as barrier band gap energy decreases, the conversion efficiency increases and the optimum efficiency obtained is 28% for an interface recombination velocity of 30 cm/s and a barrier band gap of 1.4 eV.

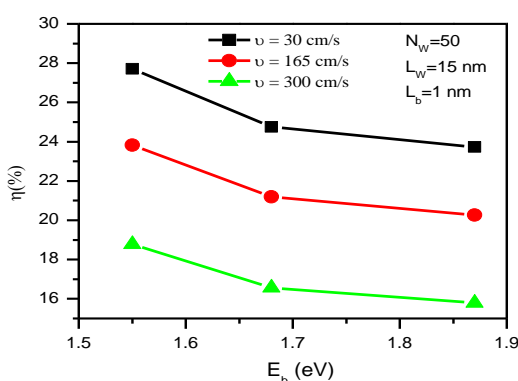


Figure 15: Dependence of the solar cell conversion efficiency on the barrier band gap energy for different interface recombination velocity

4 CONCLUSION

We have used a theoretical model, which shows that the insertion of MQW into the region a p-i(MQW)-n solar cell can significantly enhance the conversion efficiencies. Open-circuit voltages, short-circuit current densities, J-V curves and conversion efficiencies have been calculated as functions of the Al molar fractions in the barriers, width and depth of the well, number of wells in the intrinsic region and the recombination velocity in the interfaces between wells and barriers. It has been found that a considerable effect on the outputs of the cell has been obtained with the variation of the number, the depth and the width of the wells, the barrier heights (via the Al molar fraction) and widths, and the barrier-well interface recombination velocity. The doping densities however for the emitter and collector layers have slight effect. The optimized cell efficiency has reached ~29% for the lowest interface recombination velocity of 30 cm/s with 50 well in the intrinsic region.

REFERENCES

- [1] K.W.J. Barnham, G. Duggan, A new approach to high-efficiency multi-band-gap solar cells, *J. Appl. Phys.* 67(7) (1990) 3490-3493.
- [2] K.W.J. Barnham, I. Ballard, J.P. Connolly, N.J. Elkins-Daukes, B.G. Klufinger, J. Nelson, C. Rohr, Quantum well solar cells, *Physica E* 14 (1/2) (2002) 27-36.
- [3] N.G. Anderson, On quantum well solar cell efficiencies, *Physica E* 14 (1/2) (2002) 126-131.
- [4] N.G. Anderson, Ideal theory of quantum well solar cells, *J. Appl. Phys.* 78 (3) (1995) 1850-1861.
- [5] J.C. Rimada, Modelación de celdas solares p-i-n de $Al_xGa_{1-x}As$ con pozos cuánticos en la región, intrínseca MSc Thesis, Universidad de la Habana, 2000.
- [6] J. C. Rimada, L. Hernandez, J. P. Connolly, and K. W. J. Barnham, "Quantum and conversion efficiency calculation of AlGaAs/GaAs multiple quantum well solar cells" *phys. stat. sol. (b)* 242, No. 9, 1842-1845 (2005)
- [7] Stephen M. Ramey and Rahim Khoie, "Modeling of Multiple-Quantum-Well Solar Cells Including Capture, Escape, and Recombination of Photoexcited Carriers in Quantum Wells", *IEEE TRANSACTIONS ON ELECTRON DEVICES*, VOL. 50, NO. 5, MAY 2003.
- [8] F. Ragay, J. Wolter, A. Marti, and G. Araujo, "Experimental analysis of the efficiency of MQW solar cells," in *Proc. 12th Eur. Community Photovoltaic Solar Energy Conf.*, 1994, pp. 1429-1433.
- [9] F. Ragay, J. Wolter, A. Marti, and G. Araujo, "Experimental analysis of the efficiency of MQW solar cells," in *Proc. 12th Eur. Community Photovoltaic Solar Energy Conf.*, 1994, pp. 1429-1433.

- [10] J.C. Rimada, L. Hernández, A new approach to ideal AlGaAs MQW solar cells, *Mod. Phys. Lett. B* 15 (17–19) (2001) 778–781.
- [11] G. Bastard, *Wave Mechanics Applied to Semiconductor Heterostructures*, Editions de Physique, Paris, 1988.
- [12] ASTM G173-03 Standard Tables for Reference Solar Spectral Irradiances: Direct Normal and Hemispherical on 37 °C Tilted Surface, ASTM International. For referenced ASTM standards, visit the ASTM website {www.astm.org}, or contact ASTM Customer Service at service@astm.org. For Annual Book of ASTM Standards volume information, refer to the standard's Document Summary page on the ASTM website.
- [13] M. Paxman, J. Nelson, B. Braun, J.P. Connolly, K.W.J. Barnham, C.T. Foxon, J.S. Roberts, Modeling the spectral response of the quantum well solar cell, *J. Appl. Phys.* 74 (1) (1993) 614–621.
- [14] H.C. Hamaker, Computer modeling study of the effects of inhomogeneous doping and/or composition in GaAs solar cell devices, *J. Appl. Phys.* 58 (6) (1985) 2344–2351.
- [15] E.H. Li, Material parameters of InGaAsP and InAlGaAs systems for use in quantum well structures at low and room temperatures, *Physica E* 5 (2000) 215–273.